Batteries & Supercaps

Research Article
doi.org/10.1002/batt.202300196

Chemistry Europe
European Chemical Societies Publishing

www.batteries-supercaps.org

Lithium Nitrate as Salt Additive for Solid Electrolyte Interphase Formation in Dual-Ion Battery

Sandeep Das[a] and Biswarup Pathak*[a]

Tuning the solid electrolyte interphase (SEI) formation in dual-ion batteries is important for improving their long-term stability. In this context, salt additives have gained importance which can sacrificially undergo reduction thereby protecting the working salt. Herein, we have considered dual salt electrolyte models of $LiNO_3$ additive with $LiPF_6$ and LiFSI salt to carry out ab initio molecular dynamics (AIMD) simulations and witness the evolution of SEI layer. Various contact ion pair and solvent separated ion pair models of the dual salt electrolytes have been considered to further understand the role played by solvation shells of the ions. The small size and quicker diffusion of anions through the electrolyte results in its decomposition at the electrode surface irrespective of the anion being in contact ion pair or solvated by solvent molecules. Overall, along with underlining the role of salt additives in SEI formation, this detailed study also provides insights regarding the factors beyond solvation characteristics of salt that determines the SEI growth process.

Introduction

In the current scenario, lithium-ion batteries are being utilized as the major energy storage devices as we move towards harnessing renewable energy to meet the exorbitant energy demands.[1–4] However, low abundance, increasing prices of lithium, high production costs coupled with environmental hazards and safety issues have necessitated the exploration of alternate energy storage mechanisms.[5] Dual-ion batteries have thus become an attractive research area which is being developed as a safer alternative to metal ion battery.[6–8] In this case, metal anodes are used along with graphitic cathodes and the source of the ions is the electrolyte. Unlike lithium-ion batteries, both the cation and anion from solvent are involved in the battery cycling mechanism.

Other than the cycling mechanism in a dual-ion battery, solid electrolyte interphase (SEI) formation is an important phenomenon which limits or decides the longevity of the dual-ion battery. In an ideal scenario, the LUMO of the electrolyte components should be higher than the Fermi level of the anode material so that there is no charge transfer from the anode directly into the electrolyte.[9] However, the energy levels of the electrolyte get altered due to various factors resulting in the anode inducing electrolyte reduction.[10] This reduced electrolyte components along with the oxidised anode material components form the passivation layer known as SEI layer. Formation of a stable SEI is important to stop further electrolyte decomposition in the longer timescale. The electrolyte components contributing to the SEI layer could be solvent, additives, or the salt in the electrolyte.[11–13] While solvent reduction should be avoided, salt decomposition can lead to formation of an inorganic SEI layer which is more robust and potentially avoid dendrite formation.[14,15] Nevertheless, the salt is required to supply the ions to continue the battery cycling process and hence decomposition of salt is not beneficial for the electrochemical performance of the battery. Hence, salt decomposition and subsequent SEI formation though inevitable must be limited by tuning the composition of the electrolyte.

One strategy to protect the salt from getting decomposed is to add a salt additive like $LiNO_3$ which may actively participate in the SEI formation process. Thus, dual-salt electrolytes are being used recently to mitigate the uncontrolled SEI formation leading to battery failure. $LiNO_3$ has been used as one of components in various dual salt electrolytes for dual-ion batteries.[16–21] Previous studies have shown that the probability of a salt getting decomposed depends on whether it forms contact-ion pair or solvent separated ion pair in the electrolyte.[22,23] The existence of both the cation and anion in the same solvation shell (contact ion pair) leads in easier decomposition compared to when the cation and anion are solvated separately in the electrolyte (solvent separated ion pair). In case of dual-salt electrolyte the idea is to introduce a salt whose anions can participate in the Li solvation shell more strongly compared to the primary anion. In this way, the secondary anion such as $LiNO_3$ is expected to decompose preferentially over the primary anion like $LiPF_6$. However, these studies are based on understanding of the solvation shell structures of the various considered salts and solvents.[18–21] However further insights can be gained by modelling the electrode-electrolyte interphase and studying the SEI layer formation which is lacking in the case of dual-ion batteries.

Recently, a $LiNO_3$ modified carbonate-based electrolyte has been used in a $LiPF_6$ dual-ion battery to mitigate the nonuniform Li nucleation/growth because of which longer cycle life and capacity retention could be achieved.[24] There are also reports of using $LiNO_3$ as additive in ether-based solvents, but

[a] S. Das, Prof. Dr. B. Pathak
Department of Chemistry, Indian Institute of Technology (IIT) Indore, Simrol, 453552 Indore, India
E-mail: biswarup@iiti.ac.in
Homepage: https://iiti.ac.in/people/~biswarup/index.html

Supporting information for this article is available on the WWW under https://doi.org/10.1002/batt.202300196

Research Article
doi.org/10.1002/batt.202300196
Chemistry Europe
European Chemical Societies Publishing

they exhibit a lower electrochemical window.[16,25] On the other hand, this report showed that $LiNO_3$ with carbonate-based solvent can control uniform SEI deposition in a battery operating at higher voltage.[24] Lithium bis(fluorosulfonyl)imide (LiFSI) has also been used due to its ability to form a uniformly deposited SEI layer.[14,26–28] In this work we have explored the SEI formation for dual-salt electrolytes by considering $LiNO_3$ along with $LiPF_6$ and LiFSI (Scheme 1). Al anodes are found to be attractive for dual-ion battery due to features like high volumetric capacity (four times of Li), abundance and safer handling.[29–31] During battery cycling, the Li deposition/stripping on Al anodes leads to alloy (LiAl) formation.[32] As we have found in our previous works, the higher extent of decomposition in contact with LiAl than Al surface, we have considered the LiAl surface in this work.[11,12] By carrying out ab initio molecular dynamics simulations we have evaluated the applicability of various concepts like solvation shell, contact ion pair vs solvated ion pair, etc. in our models and finally to find the origin of suitability of $LiNO_3$ as a salt additive.

Computational Details

The first principles calculations have been carried out using generalized gradient approximation of Perdew Burke Ernzerhof (GGA-PBE) exchange-correlation functional.[33] All the ab initio molecular dynamics (AIMD) simulations have been carried out in CP2K package with k-point sampling at Γ-point.[34] DFT-D3 has been included to account for dispersion energy corrections.[35,36] Geodecker-Teter-Hutter (GTH) pseudopotentials have been considered for all the elements.[37–39] For Li, B, Al atoms, DZVP-MOLOPT-SR-GTH basis set has been used whereas for H, C, N, O, F, P, S atoms, TZVP-MOLOPT-SR-GTH basis set has been used. The plane wave energy cutoff was set to 500 eV. The AIMD simulations have been carried out for 20 ps with a time step of 1 fs at 350 K. The temperature was considered keeping in mind the boiling point of ethyl methyl carbonate (EMC) which is 380 K. Nosé-Hoover thermostat was considered to maintain the temperature during the simulations.[40,41] Bader charge analysis is performed using the Henkelman program to quantify and understand the charges on specific molecules.[42–45]

Four layered 3×3 supercell of (001)-terminated LiAl surface has been considered to model the lithiated alloy of Al electrode. The lattice parameters of the LiAl(001) surface is ($a=b=19.04$ Å). The electrolyte packing is done using PACKMOL software which can generate a good starting geometry based on input parameters such as types, number and position of molecules as well as minimum distance between the molecules.[46,47] The packing has been done maintaining the density of EMC solvent (1.01 g/cm^3) into the available space in the electrode model. Total number of molecules considered in the electrolyte is 15 which consists of one or two molecules of salt and the rest are EMC solvent molecules. The contact ion pair salts are represented within a square bracket ([cation anion]) whereas the solvent separated ion pairs are represented with separate square brackets ([cation][anion]). Thus, various single salt and dual salt electrolyte models considered are shown in Figure 1. The electrolyte part is first subjected to structural relaxation followed by modelling the electrolyte with LiAl surface by keeping the middle two layers fixed. For single salt models, we have only considered the contact ion pair models as they undergo faster decomposition and SEI formation compared to solvent separated pairs as established in a report using $Mg(TFSI)_2$ salt.[22] However for dual salt models we have considered possible combinations of contact ion pair as well as solvated ion pair models to unravel the underlying factors contributing towards electrolyte decomposition and SEI formation.

Results and Discussion

Here we discuss the simulation results by dividing the sections into first single salt models of $LiPF_6$, LiFSI and $LiNO_3$ followed by dual salt models of $LiPF_6$ and LiFSI with $LiNO_3$.

Single salt electrolytes

First, we have considered electrolyte models of a single salt ($LiPF_6$/LiFSI/$LiNO_3$) in the EMC solvent in contact with LiAl electrode surface. In case of [$LiPF_6$]-EMC, the simulated structure of the electrode electrolyte interphase is provided in Figure 2(a).

As is evident from the simulated structure, the $LiPF_6$ salt decomposition is not observed within the simulated time. In other words, the P–F bond distances do not change (Figure S1a). Also, the anion is found to remain within the solvent in the z-coordinate vs time plot (Figure S1a), whereas the Li is found closer to the surface after the simulation (Figure 2a). The charges on the constituent atoms of the PF_6 anion are also found to remain similar after simulation as the salt remains intact (Table S1). This reiterates the restricted participation of $LiPF_6$ in SEI formation as observed in our previous report also.[11] The charge transfer from LiAl surface to the electrolyte is calculated to be 8.65 |e| (Table S2). As the $LiPF_6$ is less prone to reduction, some EMC solvent molecules are found to get decomposed by the charge transferred from surface. Two out of 14 EMC solvent molecules are found to decompose (Figure 1a) leading to intermediates like C_2H_5OCOO, CH_3OCOO, C_2H_4, CH_2,

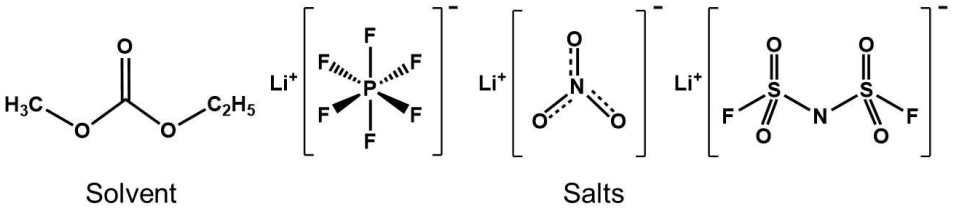

Scheme 1. Considered solvent: ethyl methyl carbonate (EMC), and salts: lithium hexafluorophosphate ($LiPF_6$), lithium nitrate ($LiNO_3$), lithium bis(fluorosulfonyl)imide) (LiFSI).

Research Article
doi.org/10.1002/batt.202300196
Chemistry Europe
European Chemical Societies Publishing

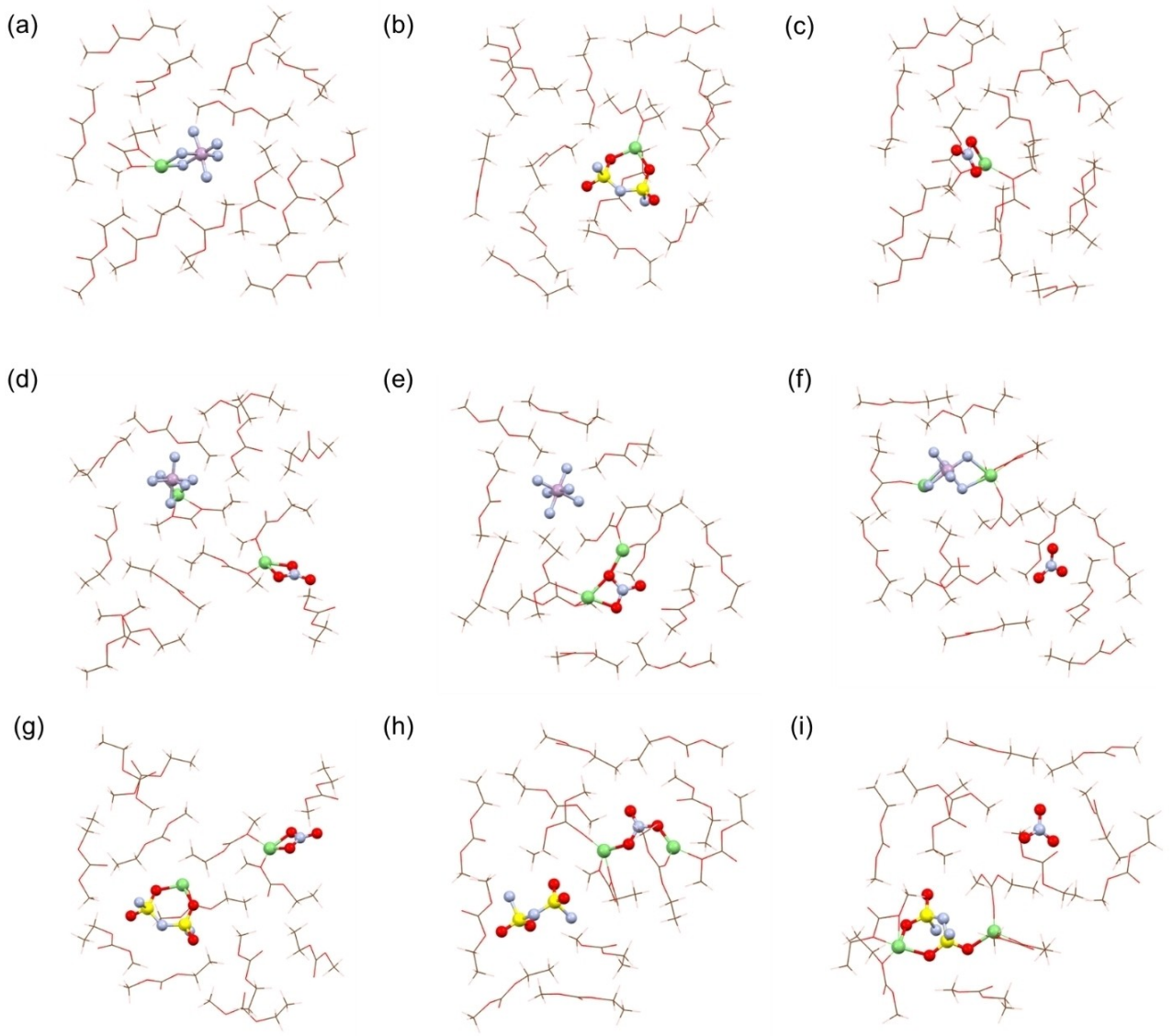

Figure 1. Considered electrolyte models: a) [$LiPF_6$]-EMC, b) [LiFSI]-EMC, c) [$LiNO_3$]-EMC, d) [$LiPF_6$]-EMC-[$LiNO_3$], e) [Li][PF_6]-EMC-[$LiNO_3$], f) [$LiPF_6$]-EMC-[Li][NO_3], g) [LiFSI]-EMC-[$LiNO_3$], h) [Li][FSI]-EMC-[$LiNO_3$], i) [LiFSI]-EMC-[Li][NO_3].

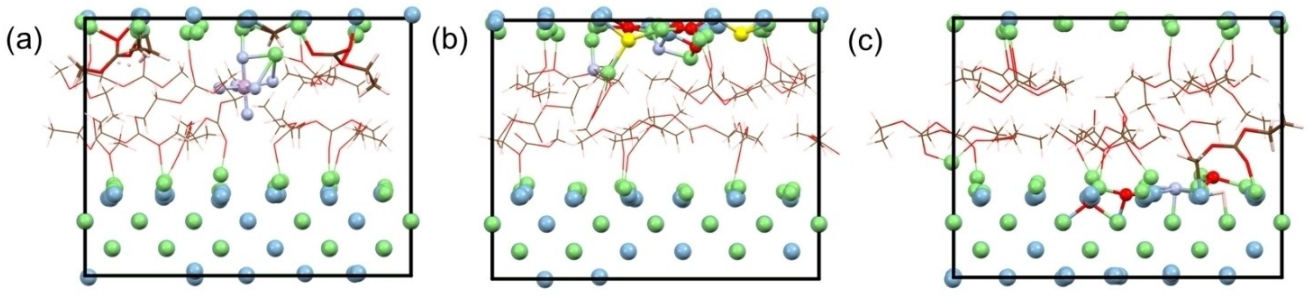

Figure 2. Electrode electrolyte interphase models for a) [$LiPF_6$]-EMC, b) [LiFSI]-EMC, c) [$LiNO_3$]-EMC, with LiAl surface after 20 ps simulation. Representation: intact solvent molecules: wireframe; decomposed solvent: capped stick; salt components: ball and stick.

and H. Thus, the SEI layer is majorly composed of EMC solvent components.

In case of electrode electrolyte model of LiFSI salt, decomposition of salt anion is observed in the simulated structure as shown in Figure 2(b). The bond distance vs time

Research Article
doi.org/10.1002/batt.202300196

plot shows that the FSI is completely decomposed (Figure S1b). The N–S and S–F bonds are broken initially followed by S–O bonds. The decomposed components (Figure 2b) are adsorbed on the LiAl surface thereby oxidizing the surface Li and Al atoms. The movement of the anion towards the surface as it gets decomposed is also evident in the z-coordinate vs time plot in Figure S1(b). The FSI decomposition and its participation in SEI is well known in literature.[14] The anion reduction is also reflected in the charges of constituent S atoms (Table S1). The charge transfer from LiAl surface is calculated to be 18.98|e| (Table S2), which is higher than the case of [$LiPF_6$]-EMC, as the FSI is completely decomposed by reduction. As the salt reduction is taking the transferred charge, the EMC solvent molecules (Figure 2b) are not found to undergo any decomposition in this case. Thus, the SEI layer is majorly inorganic in nature due to the presence of decomposed salt components and electrode surface atoms.

Moving ahead we have carried out AIMD simulation for the single salt model of [$LiNO_3$]-EMC. In this case as well, complete decomposition of NO_3 is observed in the simulated structure (Figure 2c) and bond distance vs time plot (Figure S1c). The decomposed components are found adsorbed on the surface. The anion movement is also seen in Figure S1(c) as the decomposed N and O atoms diffuse into the LiAl surface. The charge on N atom also reflects the N atom getting reduced (Table S1). The charge transfer from LiAl surface to the electrolyte is calculated to be 12.79|e| which triggers the decomposition in SEI formation (Table S2). In this case as well one EMC is found to decompose giving $C_2H_5OCOOCH_2$ and H (Figure 2c). However, the number of solvent molecules getting decomposed is less than in [$LiPF_6$]-EMC. Overall, the SEI is composed of both salt and solvent components.

We have also calculated the charge transferred required in each case for only the salt to get decomposed without the solvent getting decomposed as stability of the solvent molecules is important. The values are provided in Table S3. However, the charge transferred could not be calculated for few of the systems where the EMC solvent got decomposed before the salt as presented in the Table S3. The lowest charge transfer value of 5.10|e| obtained for [$LiNO_3$]-EMC signifies the easier reduction of NO_3 compared to FSI and PF_6. In case of [$LiPF_6$]-EMC, at a charge transfer of 12.65|e|, two solvent molecules got decomposed whereas the PF_6 salt was not found to decompose. In case of FSI as well the salt decomposition occurs at a high charge transfer value of 18.98|e| without the solvent getting decomposed. This shows that, whereas utilizing PF_6 can lead to more solvent decomposition, combination of $LiNO_3$ with LiFSI is more preferrable as they can preferentially get decomposed.

Dual salt electrolytes

Here we have considered various contact ion pair and solvated ion pair combinations of $LiPF_6$ or LiFSI with the salt additive $LiNO_3$.

$LiPF_6$ and $LiNO_3$

First, we investigate the contact ion pair system [$LiPF_6$]-EMC-[$LiNO_3$]. Here, cation and anion in both the salts are in contact with each other at the start of the simulation as represented by the electrolyte model in Figure 1(d). Upon simulating the structure, we observe SEI formation by participation of decomposed NO_3 anion as can be observed in Figure 3(a).

The PF_6 can be found to remain intact as the Li is found closer to the surface. The bond distance vs. time plot in Figure S2(a) also shows that while P–F bonds do not vary, N–O bonds change considerably indicating decomposition. The charges on PF_6 do not change much whereas the N gains charge as it is reduced during the simulation (Table S4). The distance between Li and P in $LiPF_6$ is 2.57 Å, which is higher than Li–N distance of 2.29 Å in $LiNO_3$ before the simulation. Thus, the preferable decomposition of $LiNO_3$ over $LiPF_6$ can be related to stronger interaction between Li and NO_3 (−6.69 eV) compared to Li and PF_6 (−6.08 eV). It is well reported that stronger participation of anion in the cation solvation shell leads to easier decomposition.[16,20] After getting decomposed the N adsorbs at the surface interacting with Li and Al forming compounds like Li_xAl_yN (Figure 3a). The favourable decomposition of NO_3 over PF_6 could be the reason that in experimental reports Li_3N is found to be a major component of the formed SEI layer.[16,25,48] The quicker diffusion of NO_3 towards the surface compared to that of PF_6 during the simulation could be another reason (Figure S2a). The LiAl surface is found to transfer

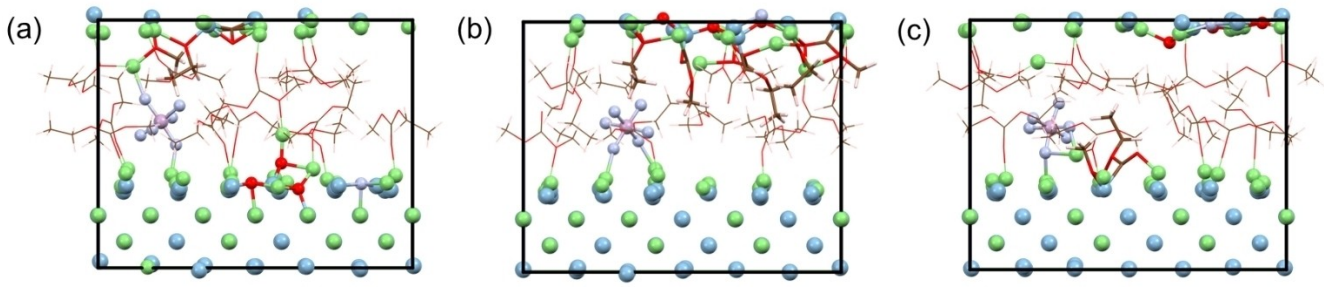

Figure 3. Electrode electrolyte interphase models for a) [$LiPF_6$]-EMC-[$LiNO_3$], b) [Li][PF_6]-EMC-[$LiNO_3$], c) [$LiPF_6$]-EMC-[Li][NO_3], with LiAl surface after 20 ps simulation. Representation: intact solvent molecules: wireframe; decomposed solvent: capped stick; salt components: ball and stick.

Research Article
doi.org/10.1002/batt.202300196
Chemistry Europe
European Chemical Societies Publishing

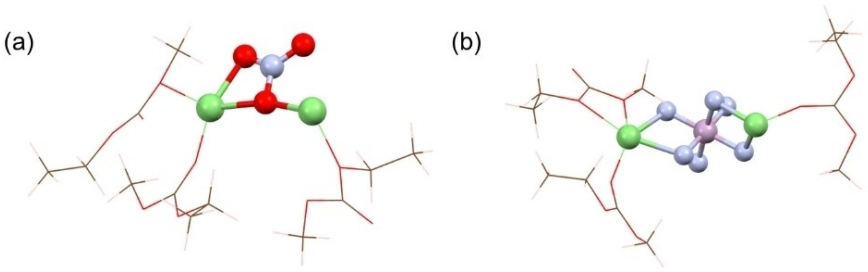

Figure 4. Solvation shell of cations in the electrolyte models of a) [Li][PF_6]-EMC-[$LiNO_3$] and b) [$LiPF_6$]-EMC-[Li][NO_3] before simulation.

15.90|e| charge to the electrolyte during simulation (Table S2). As a result of the charge transfer, other than $LiNO_3$ salt, one EMC solvent molecule is also found to decompose into C_2H_5O, CO, CH_3O fragments as can be seen in Figure 3(a). This solvent reduction is a 2-electron reduction process as observed in our previous report.[11] Thus, the formed SEI layer has both solvent and salt components. These results validate the fact that $LiNO_3$ added $LiPF_6$ in EMC solvent is a good choice for dual ion battery fabrication where the $LiPF_6$ provides working ions and $LiNO_3$ facilitates uniform SEI formation.[24]

Now, we have considered [Li][PF_6]-EMC-[$LiNO_3$] where, PF_6 part is solvated whereas the $LiNO_3$ part exist as contact ion pair. Further, the Li of PF_6 is also placed close to the $LiNO_3$ so that the PF_6 part can be solvated separately and avoid the $LiPF_6$ forming a contact ion pair (Figure 1e). After simulation, we observe that the PF_6 is still intact whereas the NO_3 gets reduced and adsorbed on the surface as is evident from Figure 3(b). The bond distance vs time plot also confirms the same (Figure S2b). The charge on N also indicate reduction of NO_3 while there is no significant change for PF_6 as is evident from Table S4. The diffusion of NO_3 towards the surface compared to that of PF_6 during the simulation is also observed (Figure S2b). The charge transfer from LiAl surface is calculated to be 17.03|e| which is more than the [$LiPF_6$]-EMC-[$LiNO_3$] model (Table S2). As a result, higher extent of solvent reduction is also observed in this case (Figure 3b). Two of the EMC molecules are found to decompose resulting in CH_3OCO, C_2H_5O, CH_3 and C_2H_5OCOO fragments. These fragments result from incomplete one-electron reduction of EMC. Thus, overall, the SEI formed in this case is composed of reduced NO_3 salt fragments and higher amount of solvent decomposed products.

Further we have evaluated the model [$LiPF_6$]-EMC-[Li][NO_3], where $LiPF_6$ is in a contact ion pair whereas NO_3 is solvated away from the Li at the start of the simulation (Figure 1f). The Li of NO_3 is placed close to $LiPF_6$ to avoid its interaction with the NO_3. In this case as well, after simulation, the NO_3 is found to decompose preferentially whereas the PF_6 remains intact as shown in Figure 3(c). The bond distance vs time plot also shows the decomposition of NO_3 (Figure S2c). As a result, the N of NO_3 gains charge as it gets reduced whereas the charges on constituent atoms of PF_6 do not vary much as is evident from Table S4. The diffusion of NO_3 as it gets reduced and thereby decomposes quickly can be seen in Figure S2(c). In this case we observe that even though PF_6 participates in the solvation shell of two Li atoms and NO_3 is only solvated by EMC solvent molecules, still the NO_3 gets reduced easily whereas the same is not true for PF_6. Thus, the theory that anions participating in solvation shell of a cation have a higher tendency to reduce does not work in all cases.[22] In our case, the small size of NO_3 and its quicker diffusion through the electrolyte takes priority as the decomposition occur only in contact with the electrode surface. Thus, the presence of salt closer to the surface is important for its actual reduction by the charge transferred from electrode surface. The charge transfer from LiAl surface to the electrolyte system is calculated to be 13.84|e| (Table S2). The less charge transfer compared to previous models also leads to less solvent decomposition as only one EMC molecule is found to undergo one-electron reduction resulting in $OCOC_2H_5$ and OCH_3 fragments (Figure 3c). Thus, the SEI layer in this case as well consists of decomposed fragments of NO_3 and one EMC solvent.

To understand the reason behind different number of EMC solvent getting reduced in [Li][PF_6]-EMC-[$LiNO_3$] and [$LiPF_6$]-EMC-[Li][NO_3] electrolyte models, we have extracted the cations and nearby solvents and anion as clusters from the electrolyte models as represented in Figure 4. We note that in case of [Li][PF_6]-EMC-[$LiNO_3$], both the reduced EMC solvents were in contact with the Li atoms, whereas in case of [$LiPF_6$]-EMC-[Li][NO_3], the one reduced EMC does not belong to the solvation shell of cations. Upon calculating the interaction energy of EMC with rest of the cluster, we find that the interaction between EMC and $Li_2PF_6(EMC)_2$ is stronger than EMC and $Li_2NO_3(EMC)_2$ (Table 1). Thus, due to weaker interaction, the EMC molecules in close vicinity of Li_2NO_3 can diffuse towards the surface and get decomposed unlike EMC molecules near Li_2PF_6.

$LiNO_3$ additive used in an EMC-$LiPF_6$ battery was reported to increase the overpotential of Li electrodeposition, thus inhibiting dendritic growth and further improve the stability of the Li metal anode.[24] Our results illustrate the sacrificial ability of NO_3

Table 1. Interaction energy for a solvent in the solvation shell of considered electrode-electrolyte models.

System	Interactions	Interaction energy [eV]
[Li][PF_6]-EMC-[$LiNO_3$]	EMC···$Li_2NO_3(EMC)_2$	−0.46
[$LiPF_6$]-EMC-[Li][NO_3]	EMC···$Li_2PF_6(EMC)_2$	−0.72

Research Article
doi.org/10.1002/batt.202300196
Chemistry Europe
European Chemical Societies Publishing

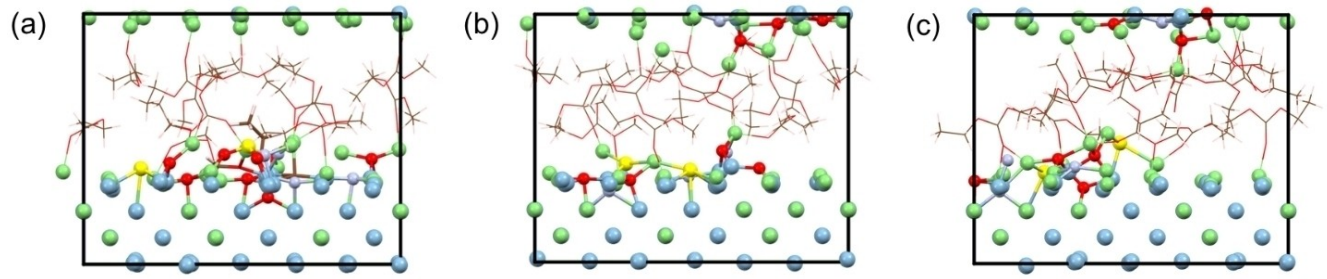

Figure 5. Electrode electrolyte interphase models for a) [LiFSI]-EMC-[$LiNO_3$], b) [Li][FSI]-EMC-[$LiNO_3$], () [LiFSI]-EMC-[Li][NO_3], with LiAl surface after 20 ps simulation. Representation: intact solvent molecules: wireframe; decomposed solvent: capped stick; salt components: ball and stick.

irrespective of its solvation behaviour, thereby contributing to the SEI formation process and hence could be the origin of improved stability of the anode surface.

LiFSI and $LiNO_3$

Moving to the dual salt mixtures of LiFSI with $LiNO_3$, we first investigate the contact ion pair system [LiFSI]-EMC-[$LiNO_3$]. Here, cation and anion in both the salts are in contact with each other at the start of the simulation as represented by the electrolyte model in Figure 1(g). After carrying out the simulation, we observe that the SEI is formed by decomposition of both the salt anions, FSI and NO_3 as represented in Figure 5(a). The bond distance vs time plots in Figure S3(a) show that the NO_3 is completely decomposed upon reduction. For FSI, though the N–S and S–F bonds start breaking in the initial steps, complete decomposition is not observed. Some of the bond distances are found to remain constant throughout the simulation thereby signifying incomplete reduction (Figure S3a). The incomplete decomposition is also reflected in the Bader charge values as there is uneven loss/gain in charge among the two S atoms (Table S5). On the other hand, complete decomposition of NO_3 is also reflected in the charge gained by N atom. This can be explained by stronger interaction between Li and NO_3 (−6.69 eV) compared to Li and FSI (−6.20 eV). Also, the distance between Li and N in FSI (3.31 Å) is higher than that of Li and NO_3 (2.28 Å). Thus, stronger participation of NO_3 in the cation solvation shell facilitates its complete decomposition. The diffusion of NO_3 towards the surface is also quicker compared to FSI triggering its decomposition (Figure S3a). The charge transfer from the LiAl surface during the simulation is calculated to be 28.98|e| (Table S2). As a result of the charge transfer, one EMC solvent molecule is found to decompose into OC_2H_5, OCH_3, C and O fragments (Figure 5a). Thus, the SEI layer is composed of fragments originating from both salts and one EMC solvent molecule.

Further we have considered [Li][FSI]-EMC-[$LiNO_3$], where FSI is solvated in the EMC solvent while $LiNO_3$ exists as contact ion pair (Figure 1h). Like in [Li][PF_6]-EMC-[$LiNO_3$], here as well the Li of FSI is placed close to $LiNO_3$ at the start of the simulation. After the simulation, we observe that both the anions are decomposed as shown in Figure 5(b). The bond distance vs time plot also shows that all the N–O bonds in NO_3 are broken followed by the bonds in FSI during the simulation (Figure S3b). The FSI is also found to decompose completely in this electrolyte model. This is also reflected in both the S atoms gaining similar charge after decomposition (Table S5). The diffusion of NO_3 towards the surface is found to occur quicker than diffusion of FSI which triggers the preferential reduction of NO_3 before FSI (Figure S3b). The fact that NO_3 participates in the solvation shell of Li cations could also play a role in its preferable bond dissociations before FSI. The charge transfer from LiAl surface to the electrolyte is calculated to be 26.94|e| (Table S2). Interestingly all the EMC solvent molecules remain intact in this case thereby achieving a solely inorganic component derived SEI layer (Figure 5b).

Lastly, we study the changes in [LiFSI]-EMC-[Li][NO_3] electrolyte model as illustrated in Figure 1(i). Here, the Li of NO_3 salt is placed close to LiFSI such that the NO_3 is solvated before the simulation. Both the FSI and NO_3 are found to get reduced and decompose during the simulation (Figure 5c). The bond distance vs time plot shows that the S–F bond of FSI along with the NO_3 start breaking early and the whole salts get decomposed during the simulation (Figure S3c). Once again, the NO_3 is found to undergo complete decomposition before the FSI (Figure S3c). The presence of FSI in the Li cation solvation shell may be the reason that FSI decomposition process starts early along with NO_3. However, with quicker diffusion due to small size, NO_3 decomposition is completed early compared to FSI. Also, the diffusion of NO_3 towards the surface is completed before that of FSI as can be seen in the z-coordinate vs time plot in Figure S3(c). Moreover, the change in charges on constituent atoms of both the salts also show the complete decomposition (Table S5). 26.69|e| charge is found to be transferred from surface to the electrolyte (Table S2). None of the EMC solvent molecules are decomposed during the simulation. Hence, the SEI layer formed consists of only inorganic components from both the salts. LiFSI along with $LiNO_3$ are found to form a stable SEI layer in experimental reports, thereby increasing stability of the Li anode in the battery.[18,49] This could be due to the complete decomposition of both the salts observed in the solvated salt models involving LiFSI and $LiNO_3$, along with absence of solvent decomposition which leads to an inorganic component composed uniform and stable SEI layer.

Conclusions

In this work, we have carried out a detailed study on the applicability of $LiNO_3$ as a salt additive in electrolyte which sacrifices itself in solid electrolyte interphase (SEI) formation, thereby protecting the working components of the battery. Various configurations (contact ion pair and solvent separated ion pair) of mixture of $LiPF_6$/LiFSI salt with $LiNO_3$ salt additive is considered along with EMC solvent for AIMD simulations in contact with LiAl surface to gain insights into the SEI layer formation process. In case of dual salt electrolyte models of $LiPF_6$ and $LiNO_3$, NO_3 is found to decompose irrespective of it being solvated together with cations or only solvent. $LiPF_6$ decomposition is not observed within the timescale of simulations carried out. For dual salt electrolyte models involving LiFSI and $LiNO_3$, both the salts are found to undergo decomposition but the NO_3 is found to undergo complete and quicker decomposition preferentially over FSI. Though FSI starts decomposition at similar time scale with NO_3 when it is present in the solvation shell of cation, the complete decomposition of NO_3 occurs earlier. The decomposition trends in case of cation pair salt models agree with the interaction energy trends between cation and the different anions. Overall, the smaller size of NO_3 leading to its easier diffusion through the solvent towards the surface is found to play a major role in its preferential decomposition as the SEI formation process occurs in contact with the electrode surface. Also, absence of EMC solvent decomposition in the solvent separated ion pair models of LiFSI with $LiNO_3$ show their suitability as the most preferred combinations for dual ion battery from the SEI formation perspective. Overall, this work signifies how the solvation environment as well as nature of the considered salt can tune the SEI formation process.

Supporting Information

The supporting information file contents are bond distance vs time plots, position vs time plots, charge transferred from electrode to electrolyte and charges on anions for the considered dual salt electrolyte models.

Acknowledgements

We thank IIT Indore for lab and computing facilities. This work is supported by DST-SERB (Project Number CRG/2018/001131; CRG/2022/000836), and CSIR (Project Number 01(3046)/21/EMR-II). S. D. thanks CSIR for research fellowship.

Conflict of Interests

The authors declare no conflict of interest.

Data Availability Statement

The data that support the findings of this study are available in the supplementary material of this article.

Keywords: solid electrolyte interphase · salt additive · $LiNO_3$ · $LiPF_6$ · LiFSI · ethyl methyl carbonate

[1] B. Dunn, H. Kamath, J. M. Tarascon, *Science* **2011**, *334*, 928–935.
[2] Z. Yang, J. Zhang, M. C. W. Kintner-Meyer, X. Lu, D. Choi, J. P. Lemmon, J. Liu, *Chem. Rev.* **2011**, *111*, 3577–3613.
[3] N. Nitta, F. Wu, J. T. Lee, G. Yushin, *Mater. Today* **2015**, *18*, 252–264.
[4] J. M. Tarascon, *Nat. Chem.* **2010**, *2*, 510–510.
[5] J. M. Tarascon, M. Armand, *Nature* **2001**, *414*, 359–367.
[6] M. Wang, Y. Tang, *Adv. Energy Mater.* **2018**, *8*, 1703320.
[7] S. Das, S. S. Manna, B. Pathak, *ChemSusChem* **2023**, *16*, e202201405.
[8] S. Das, S. S. Manna, B. Pathak, *ACS Omega* **2021**, *6*, 1043–1053.
[9] J. B. Goodenough, Y. Kim, *Chem. Mater.* **2010**, *22*, 587–603.
[10] S. A. Delp, O. Borodin, M. Olguin, C. G. Eisner, J. L. Allen, T. R. Jow, *Electrochim. Acta* **2016**, *209*, 498–510.
[11] S. Das, P. Bhauriyal, B. Pathak, *J. Phys. Chem. C* **2020**, *124*, 7634–7643.
[12] S. Das, S. S. Manna, B. Pathak, *ACS Appl. Energ. Mater.* **2022**, *5*, 13398–13409.
[13] S. Das, B. Pathak, *ACS Appl. Energ. Mater.* **2023**, *6*, 6041–6050.
[14] L. E. Camacho-Forero, T. W. Smith, P. B. Balbuena, *J. Phys. Chem. C* **2017**, *121*, 182–194.
[15] X. Zhou, Q. Zhang, Z. Zhu, Y. Cai, H. Li, F. Li, *Angew. Chem. Int. Ed.* **2022**, *61*, e202205045.
[16] S. Zhang, G. Yang, Z. Liu, X. Li, X. Wang, R. Chen, F. Wu, Z. Wang, L. Chen, *Nano Lett.* **2021**, *21*, 3310–3317.
[17] S. Kim, T. K. Lee, S. K. Kwak, N. S. Choi, *ACS Energy Lett.* **2022**, *7*, 67–69.
[18] X. Q. Zhang, X. Chen, L. P. Hou, B. Q. Li, X. B. Cheng, J. Q. Huang, Q. Zhang, *ACS Energy Lett.* **2019**, *4*, 411–416.
[19] Z. Wang, Y. Wang, B. Li, J. C. Bouwer, K. Davey, J. Lu, Z. Guo, *Angew. Chem. Int. Ed.* **2022**, *61*, e202206682.
[20] Z. Piao, P. Xiao, R. Luo, J. Ma, R. Gao, C. Li, J. Tan, K. Yu, G. Zhou, H. M. Cheng, *Adv. Mater.* **2022**, *34*, 2108400.
[21] Z. Wen, W. Fang, X. Wu, Z. Qin, H. Kang, L. Chen, N. Zhang, X. Liu, G. Chen, *Adv. Funct. Mater.* **2022**, *32*, 2204768.
[22] G. Agarwal, J. D. Howard, V. Prabhakaran, G. E. Johnson, V. Murugesan, K. T. Mueller, L. A. Curtiss, R. S. Assary, *ACS Appl. Mater. Interfaces* **2021**, *13*, 38816–38825.
[23] Y. Huang, B. Wen, Z. Jiang, F. Li, *Nano Res.* **2023**, *16*, 8072–8081.
[24] L. N. Wu, J. Peng, Y. K. Sun, F. M. Han, Y. F. Wen, C. G. Shi, J. J. Fan, L. Huang, J. T. Li, S. G. Sun, *ACS Appl. Mater. Interfaces* **2019**, *11*, 18504–18510.
[25] J. Zhou, J. Chen, J. Yang, Y. Nuli, J. Wang, *ACS Appl. Energ. Mater.* **2021**, *4*, 11336–11342.
[26] T. D. Pham, A. Bin Faheem, K. K. Lee, *Small* **2021**, *17*, 2103375.
[27] T. Ma, Y. Ni, Q. Wang, W. Zhang, S. Jin, S. Zheng, X. Yang, Y. Hou, Z. Tao, J. Chen, *Angew. Chem. Int. Ed.* **2022**, *61*, e202207927.
[28] J. Zhou, X. Lian, Q. Shi, Y. Liu, X. Yang, A. Bachmatiuk, L. Liu, J. Sun, R. Yang, J.-H. Choi, M. H. Rummeli, *Adv. Energy Sustain. Res.* **2022**, *3*, 2100140.
[29] Q. Li, N. J. Bjerrum, *J. Power Sources* **2002**, *110*, 1–10.
[30] N. S. Hudak, *J. Phys. Chem. C* **2014**, *118*, 5203–5215.
[31] A. A. Yaroshevsky, *Geochem. Int.* **2006**, *44*, 48–55.
[32] X. Zhang, Y. Tang, F. Zhang, C. S. Lee, *Adv. Energy Mater.* **2016**, *6*, 1502588.
[33] J. P. Perdew, K. Burke, M. Ernzerhof, *Phys. Rev. Lett.* **1996**, *77*, 3865.
[34] J. Hutter, M. Iannuzzi, F. Schiffmann, J. Vandevondele, *Wiley Interdiscip. Rev.: Comput. Mol. Sci.* **2014**, *4*, 15–25.
[35] S. Grimme, J. Antony, S. Ehrlich, H. Krieg, *J. Chem. Phys.* **2010**, *132*, 154104.
[36] S. Grimme, S. Ehrlich, L. Goerigk, *J. Comput. Chem.* **2011**, *32*, 1456–1465.
[37] S. Goedecker, M. Teter, *Phys. Rev. B* **1996**, *54*, 1703.
[38] C. Hartwigsen, S. Goedecker, J. Hutter, *Phys. Rev. B* **1998**, *58*, 3641.
[39] M. Krack, *Theor. Chem. Acc.* **2005**, *114*, 145–152.
[40] S. Nosé, *Mol. Phys.* **1984**, *52*, 255–268.
[41] W. G. Hoover, *Phys. Rev. A: At. Mol., Opt. Phys.* **1985**, *31*, 1695.
[42] R. F. W. Bader, *Chem. Rev.* **1991**, *91*, 893–928.

[43] G. Henkelman, A. Arnaldsson, H. Jónsson, *Comput. Mater. Sci.* **2006**, *36*, 354–360.
[44] E. Sanville, S. D. Kenny, R. Smith, G. Henkelman, *J. Comput. Chem.* **2007**, *28*, 899–908.
[45] W. Tang, E. Sanville, G. Henkelman, *J. Phys. Condens. Matter.* **2009**, *21*, 084204.
[46] J. M. Martínez, L. Martínez, *J. Comput. Chem.* **2003**, *24*, 819–825.
[47] L. Martinez, R. Andrade, E. G. Birgin, J. M. Martínez, *J. Comput. Chem.* **2009**, *30*, 2157–2164.
[48] D. Liu, X. Xiong, Q. Liang, X. Wu, H. Fu, *Chem. Commun.* **2021**, *57*, 9232–9235.
[49] F. Qiu, X. Li, H. Deng, D. Wang, X. Mu, P. He, H. Zhou, F. Qiu, D. Wang, X. Mu, P. He, H. Zhou, X. Li, H. Deng, *Adv. Energy Mater.* **2019**, *9*, 1803372.

Manuscript received: May 11, 2023
Revised manuscript received: July 27, 2023
Accepted manuscript online: August 7, 2023
Version of record online: August 14, 2023